


# Intermediate structural state in $\text{Bi}_{1-x}\text{Pr}_x\text{FeO}_3$ ceramics at the rhombohedral–orthorhombic phase boundary

D. V. Karpinsky<sup>1,\*</sup> , I. O. Troyanchuk<sup>1</sup>, M. Willinger<sup>2</sup>, V. A. Khomchenko<sup>3</sup>, A. N. Salak<sup>4</sup>, V. Sikolenko<sup>5</sup>, and M. V. Silibin<sup>6</sup>

<sup>1</sup> Scientific-Practical Materials Research Centre of NAS of Belarus, P. Brovka Str. 19, 220072 Minsk, Belarus

<sup>2</sup> Abteilung Anorganische Chemie, Fritz-Haber-Institut der Max-Planck-Gesellschaft, Faradayweg 4-6, 14195 Berlin, Germany

<sup>3</sup> CFisUC, Department of Physics, University of Coimbra, 3004-516 Coimbra, Portugal

<sup>4</sup> Department of Materials and Ceramics Engineering, University of Aveiro, 3810-193 Aveiro, Portugal

<sup>5</sup> Joint Institute for Nuclear Research, Dubna, Russia 141980

<sup>6</sup> National Research University of Electronic Technology "MIET", Zelenograd, Moscow, Russia 124498

---

## ABSTRACT

Crystal structure of the  $\text{Bi}_{1-x}\text{Pr}_x\text{FeO}_3$  ceramics of the compositions corresponding to the threshold concentrations separating the polar rhombohedral (R3c) and anti-polar orthorhombic (Pbam) phases has been investigated with X-ray diffraction, transmission electron microscopy and differential scanning calorimetry measurements performed in a broad temperature range. The structural study specifies the peculiarities of the temperature-driven transition into the non-polar orthorhombic (Pnma) phase depending on the structural state of the compounds at room temperature. The crystal structure analysis reveals the revival of the anti-polar orthorhombic phase upon the temperature-induced transition, thus assuming that it can be considered as the bridge phase between the polar rhombohedral and the non-polar orthorhombic phases.

---

## Introduction

Solid solutions of bismuth ferrite attract persistent scientific interest due to the multiple composition-driven structural transitions which dramatically affect the multiferroic behavior. Near the morphotropic phase boundaries, these materials are characterized by the enhanced physical properties associated with the specific structural state. It is assumed that the enhanced responses are caused by a coexistence of the adjacent-phase structural clusters with a typical size

reduced down to a nanoscale level. Such structural state is highly defective because of the numerous dislocations, inhomogeneous stress distribution, local variations of the chemical composition, etc. [1–5], which reduce its thermodynamic stability and enhance sensitivity to the external stimuli—temperature, electric/magnetic field, mechanical stress.

In  $\text{BiFeO}_3$ , chemical replacement of  $\text{Bi}^{3+}$  with the rare-earth elements possessing comparable ionic radii ( $\text{La}^{3+}$ – $\text{Eu}^{3+}$ ) causes the concentration-driven structural transition from the polar rhombohedral to the

---

Address correspondence to E-mail: [karpinski@ua.pt](mailto:karpinski@ua.pt)

non-polar orthorhombic phase that occurs via the formation of the anti-polar orthorhombic structure [4, 6–10]. Most promising physical parameters were obtained for the lanthanum and praseodymium-doped compounds within the morphotropic phase boundary region [3, 11, 12], and the phase coexistence range estimated for these compounds is stable over a very broad compositional range ( $\Delta x \sim 5\%$ ) far exceeding those attributed to the compounds doped with other rare-earth elements [4, 7]. It should be noted that the wide phase coexistence range facilitates the structural analysis of this region. It is known that the phase transition sequence is largely dependent on the substituting elements, e.g., chemical substitution by rare-earth elements with smaller ionic radii reduces the dopant concentration level triggering the structural transformation, while the width of the phase coexistence region shrinks [4, 13–16].

Recent investigations of rare-earth-doped  $\text{BiFeO}_3$  compounds prepared by different methods have testified certain difference in the structural parameters and dopant concentrations near the phase transition regions [15, 17–21]. The obtained results have specified the crystal structure peculiarities upon composition-driven transitions depending on the synthesis conditions and dopant ions. Despite on different synthesis methods, the crystal structure of the compounds  $\text{Bi}_{1-x}\text{RE}_x\text{FeO}_3$  ( $\text{RE} = \text{La}, \text{Nd}, \text{Pr}$ ) is characterized by a rhombohedral–orthorhombic phase transition within the dopant concentration range of  $0.1 < x < 0.2$ . Structural measurements taken for the rare-earth-doped  $\text{BiFeO}_3$  compounds as a function of temperature have revealed a complex evolution of the structural phases depending on the crystal structure stable at room temperature [7, 14]. The compounds characterized by the rhombohedral distortion of the unit cell at room temperature demonstrate gradual transition into the non-polar orthorhombic phase that occurs via the formation of a mixed (polar and non-polar) structural state. Within the compositional range corresponding to a coexistence of the polar and anti-polar phases, a gradual reduction in the anti-polar orthorhombic phase (accompanied by a proportional increase in the amount of the rhombohedral phase) takes place with a temperature increase. At higher temperatures, the anti-polar phase disappears and the new phase with non-polar orthorhombic structure emerges. Further temperature increase stabilizes a single-phase structural state with the non-polar orthorhombic structure. Ceramics with the major anti-

polar phase or single-phase anti-polar structure show gradual transition to the non-polar orthorhombic structure through the two-phase structural state. In the compounds having minority of the rhombohedral phase, the anti-polar phase vanishes at temperatures below that attributed to the appearance of the non-polar orthorhombic phase, so such transition is also characterized by two-phase coexistence region without any intermediate phases.

Our recent structural study of the Pr-doped compounds [22] within the phase coexistence region has revealed an intriguing evolution of the crystal structure with temperature. The structural measurements taken for the compounds with dominant rhombohedral phase at room temperature show the three-phase coexistent region stable in the narrow temperature range. It was considered that this thermodynamically non-equilibrium state is realized during the temperature-driven transformation of the anti-polar orthorhombic phase into the orthorhombic non-polar phase, while the rhombohedral phase remains notable.

Analysis of the composition- and temperature-driven structural transitions observed in the rare-earth-doped  $\text{BiFeO}_3$  compounds suggests the anti-polar orthorhombic phase to be the intermediate one between the more stable polar rhombohedral and the non-polar orthorhombic phases. The present study focuses on the clarification of the structural evolution of the Pr-doped compounds in the vicinity of the phase boundary region. Analysis of the crystal structure of the compounds across the phase transitions is crucial to determine the origin of the enhanced physical properties observed in these compounds. Declared issue is a complex technological and scientific task as there are different factors which hamper the structural analysis (i.e., limited resolution of laboratory diffractometers, mechanical stress, local defects and vacancies, etc., which locally modify the crystal structure). In order to determine the crystal structure evolution across the phase transitions, we have performed the combined microscopic (X-ray diffraction) and local scale (transmission electron microscopy) structural measurements.

## Experimental

Ceramic samples of  $\text{Bi}_{1-x}\text{Pr}_x\text{FeO}_3$  system with the dopant concentrations  $0.1 \leq x \leq 0.3$  were prepared by a two-stage solid-state reaction method [4]. High-

purity oxides taken in a stoichiometric ratio were thoroughly mixed using a planetary ball mill (Retsch PM 100). The ceramics were synthesized at temperatures in the range of 930–1030 °C (synthesis temperature was increased with a step of  $\sim 5$  °C per each percent of praseodymium content increase) followed by a fast cooling down to room temperature. X-ray diffraction measurements were taken with a PANalytical X'Pert MPD PRO diffractometer (Cu- $K_\alpha$  radiation) equipped with a heating stage (Anton Paar, HTK 16N). Diffraction data were analyzed by the Rietveld method using the FullProf software package [23]. High-resolution transmission electron microscopy (HRTEM) measurements have been taken using an FEI aberration-corrected Titan 80–300 microscope operated at 300 kV equipped with an EDX detector. Differential thermal analysis and differential scanning calorimetry were carried out with a differential scanning calorimeter Setaram (Caluire, France) in a flowing argon atmosphere.

## Results and discussion

### Crystal structure evolution across the concentration-driven transition

XRD measurements taken for the  $\text{Bi}_{1-x}\text{Pr}_x\text{FeO}_3$  solid solutions at room temperature have determined the concentration regions specific to different structural phases. It is known [9, 15, 24] that the crystal structure of the compounds with the dopant concentrations of up to  $x = 0.1$  is characterized by the polar rhombohedral phase and the obtained XRD patterns of the compound  $x = 0.1$  are in accordance with the available data. In the concentration range of  $0.11 \leq x \leq 0.15$ , the crystal structure of the compounds is characterized by a coexistence of the polar rhombohedral ( $R$ -phase) and anti-polar orthorhombic ( $O_2$ -phase) phases (Fig. 1). The anti-polar orthorhombic structure has been refined utilizing space group  $Pnam$  with a lattice metric of  $\sqrt{2}a_p \times 2\sqrt{2}a_p \times 4a_p$  ( $a_p$  is the fundamental perovskite lattice parameter). The anti-polar unit cell is similar to that observed in the anti-ferroelectric lead zirconate [25, 26]. Praseodymium doping leads to the increase in the orthorhombic phase fraction at the expense of the rhombohedral one (Fig. 2). It should be noted that a quadrupling of the  $c$ -axis weakens upon doping and it can hardly be determined in the compounds

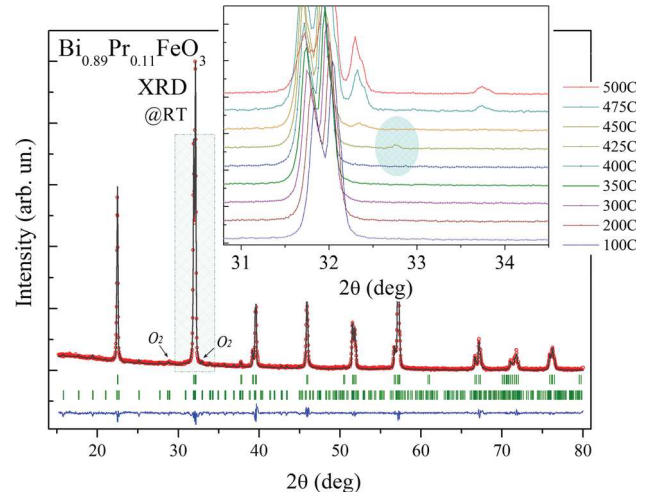


**Figure 1** XRD pattern of the  $\text{Bi}_{0.89}\text{Pr}_{0.11}\text{FeO}_3$  compound obtained at room temperature. Bragg positions attributed to the rhombohedral (*upper*) and the orthorhombic phases are marked by *vertical ticks*. The *inset* shows an evolution of the structural peaks; tiny peak attributed to the anti-polar phase is *highlighted*; the peaks attributed to the  $O_2$ -phase are marked by *arrows*.

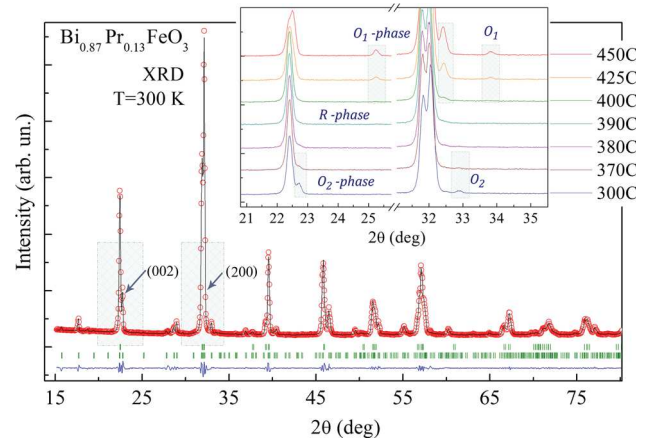


**Figure 2** XRD pattern of the  $\text{Bi}_{0.87}\text{Pr}_{0.13}\text{FeO}_3$  compound. Bragg positions attributed to the polar rhombohedral (*upper*) and the anti-polar orthorhombic phases are marked by *vertical ticks*. The *inset* shows an evolution of the structural peaks; the peaks attributed to either anti-polar or non-polar phases are denoted, the  $R$ -phase is stable over the denoted temperature range.

with  $x > 0.2$ . The unit cell is characterized by a doubled  $c$ -parameter (as compared to the fundamental perovskite structure), and the crystal structure can be successfully described by space group  $Pbam$  with metric of  $\sqrt{2}a_p \times 2\sqrt{2}a_p \times 2a_p$ . Increase in the dopant concentration leads to a stabilization of the single-phase anti-polar orthorhombic structure

(O<sub>2</sub>-phase), further chemical doping leads to a stabilization of the two-phase region followed by the single-phase state with the non-polar orthorhombic structure (space group *Pbnm*, O<sub>1</sub>-phase).

The declared structural data generally correspond to the previously published results [22, 27] while there are some minor differences which concern the two-phase concentration regions and the doping levels critical for the phase transition between the orthorhombic phases. It should be noted that the concentration ranges of the phase stability significantly depend on the synthesis conditions and the post-synthesis treatment (quenching, annealing in gaseous atmospheres, etc.). Depending on the mentioned factors, the phase boundary regions can vary within several percents [4, 15, 27, 24]. In the present study, we declare ~4% width of the rhombohedral-orthorhombic two-phase region which is quite narrow as compared to those reported so far [27, 28].

The anti-polar phase can be considered as the intermediate phase within the structural transition from the rhombohedral to the orthorhombic phase driven by chemical substitution for compounds doped with large rare-earth ions La–Eu. The structural transition in the compounds with smaller dopant ions is associated with direct structural transformation to the non-polar orthorhombic phase [15]. It is known that the concentration of the dopants and the width of the two-phase regions significantly depend on the ionic radius of substituting element. Thus, the crystal structure of the BiFeO<sub>3</sub> compounds doped with lanthanum ions is characterized by smaller changes in the structural parameters upon the chemical doping as compared to those observed in the Pr-doped samples [9]; this fact justifies a larger concentration of the substituents required to induce the structural transitions as well as a wider range of the two-phase regions. In contrast, a substitution of bismuth ions by rare-earth ions with smaller ionic radii reduces the doping level critical for the structural transition and leads to a shrinkage of the two-phase region [4, 15]. Thus, one can consider a crucial role of the size effect in the structural phase transitions observed for the doped BiFeO<sub>3</sub> compounds.

Chemical doping with praseodymium ions leads to a gradual reduction in the unit cell parameters. The unit cell volume drastically changes while passing across the phase transitions, viz., the rhombohedral-orthorhombic phase transformation is accompanied by ~0.5% change in the unit cell volume, and the

orthorhombic-orthorhombic transition is accompanied with ~1% change in the unit cell volume (Fig. 3, right image). The diffraction data reveal a significant change in the unit cell parameters across the phase transition when the phase ratio evolution testifies a gradual transformation from one phase into the other without any intermediate phase. The crystal structure analysis reveals a minor amount of the anti-polar orthorhombic phase (about 5%) in the compound with  $x = 11\%$ . The crystal structure of the compound with  $x = 0.13$  is considered to have nearly equal amount of the rhombohedral and anti-polar orthorhombic phases (Fig. 2). The compound with  $x = 15\%$  is on the other side of the phase boundary and contains about 5% of the rhombohedral phase.

The mentioned compounds represent the doping-driven structural transition from the polar rhombohedral to the anti-polar orthorhombic phase that happens without formation of any intermediate phase. The temperature-driven evolution of the crystal structure resembles that caused by the chemical substitution, while the route of the phase transformation is doubtful and it is strongly dependent on the initial structural state [9, 14]. The question about the phase coexistence in these compounds upon the temperature increase as well as a possibility of stabilization of the intermediate phase is still under discussion, so the thermal behavior of the compounds within the phase boundary region is worthy to be studied in detail.

### Temperature-driven evolution of the crystal structure

The substitution-driven structural evolution described for the Bi<sub>1-x</sub>RE<sub>x</sub>FeO<sub>3</sub> compounds is quite similar to that observed for them upon the temperature increase. The crystal structure of the Bi<sub>1-x</sub>RE<sub>x</sub>FeO<sub>3</sub> ceramics transforms into the non-polar orthorhombic one upon the temperature increase regardless the initial structural state estimated at room temperature. For the pristine BiFeO<sub>3</sub>, the rhombohedral-orthorhombic transition occurs at  $T \sim 830$  °C and is accompanied by drastic (~1.5%) decrease in the unit cell volume [29]. The BiFeO<sub>3</sub>-based compounds doped with different rare-earth ions also show transformation into the non-polar orthorhombic state, while the route of the structural evolution varies for the dopant ions and strongly depends on the structural state stable at room temperature.

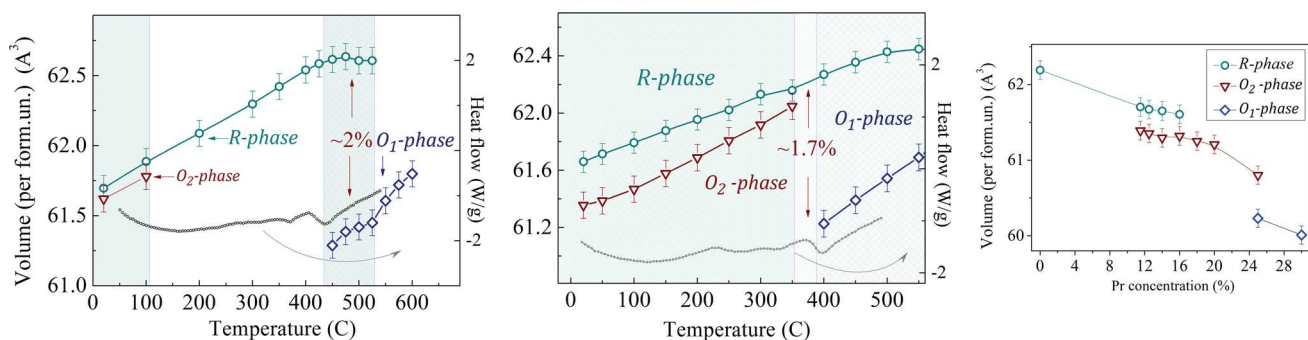


**Figure 3** Left and middle images show a temperature evolution of the unit cell volume attributed to the different structural phases calculated for the compounds with  $x = 0.11$  and  $x = 0.13$  as well

as related DSC dependences (heating curves). The right image shows an evolution of the unit cell volume as a function of praseodymium concentration.

Among the  $\text{BiFeO}_3$ -based materials doped with rare-earth elements, the solid solutions with praseodymium ions show the most intriguing evolution of the crystal structure as a function of temperature. For instance, the existence of the three-phase region has been declared for the Pr-doped compounds at temperatures about  $380^\circ\text{C}$  [10]. The authors have justified this triple point in terms of thermodynamically non-equilibrium state. The obtained structural data specify a number of structural transitions occurred in a narrow temperature range as well as the phase coexistence regions. To clarify the peculiarities of the temperature-driven structural transitions, we have thoroughly studied the compounds within the rhombohedral–orthorhombic phase boundary. It should be noted that, in contrast to the La-doped compounds, Pr-containing solid solutions do not show any structural relaxation, thus allowing an accurate study of the crystal structure evolution.

The detailed structural investigations have been performed for the samples with  $x = 0.11$ ,  $0.13$  and  $x = 0.15$ . The compounds represent nearly entire range of the morphotropic phase boundary containing the rhombohedral and the orthorhombic phases at room temperature. The structural data obtained for the compound with  $x = 0.11$  demonstrate a negligible amount of the orthorhombic phase which completely disappears at temperatures above  $100^\circ\text{C}$  (Fig. 1). The unit cell parameters of the rhombohedral phase and the unit cell volume show a gradual expansion with increasing temperature up to the temperature of the structural transition into the non-polar orthorhombic phase ( $T \sim 450^\circ\text{C}$ ). Above this temperature, the unit cell volume remains nearly constant up to the temperature of about  $520^\circ\text{C}$ , where the rhombohedral phase disappears. The unit

cell volume calculated for the non-polar orthorhombic phase gradually increases with temperature. The compound is characterized by two-phase coexistence region of about  $80^\circ\text{C}$ . At the temperatures about  $450^\circ\text{C}$  (Fig. 1, inset), one can distinguish the traces of the non-polar orthorhombic phase and the crystal structure of the compound becomes single-phase orthorhombic at temperature of about  $520^\circ\text{C}$ ; quite narrow temperature region of the two-phase structural state (about  $80^\circ\text{C}$ ) testifies the high structural homogeneity of the material.

The analysis of the XRD temperature data obtained for the compound with  $x = 0.13$  reveals a gradual increase in the lattice parameters within the measured temperature range while the phase ratio significantly changes. Nearly equal amounts of the rhombohedral and the anti-polar orthorhombic phases estimated at room temperature changes in favor of the rhombohedral phase upon temperature increase. At temperature of  $300^\circ\text{C}$ , the amount of the anti-polar phase is about 20% and it completely disappears at about  $400^\circ\text{C}$ . The new non-polar orthorhombic phase ( $O_1$ -phase) appears at  $400^\circ\text{C}$  and has been successfully refined using a centrosymmetric space group  $\text{Pnma}$ . The structural data testify a stabilization of the single-phase rhombohedral state at temperatures about  $380^\circ\text{C}$ . In spite of the single-phase state estimated from the diffraction results we cannot exclude an existence of a small amount ( $\sim 2\text{--}3\%$ ) of the anti-polar phase with spatial size of nanoscale level.

The unit cell parameters attributed to the rhombohedral and the non-polar orthorhombic structural phases gradually increase with temperature up to  $550^\circ\text{C}$ . The structural transition into the non-polar orthorhombic phase can be considered as a

transformation of anti-polar orthorhombic structure to the non-polar orthorhombic one associated with a reduction in the amount of the former phase and evidently its crystalline volume down to the nanoscale sizes. This transition is quite different as compared with that occurred in the compound with  $x = 0.11$  while the related anomalies at the DSC curves are quite similar.

In order to complete the picture of the temperature-driven structural transition into the non-polar orthorhombic phase depending on the structural state stable at room temperature, we have also traced a structural evolution of the compound with  $x = 0.15$ . The crystal structure of this compound is characterized by single-phase anti-polar orthorhombic structure above 100 °C. The additional diffraction peaks observed in the XRD pattern at 375 °C belong to the new structural phase with the non-polar orthorhombic structure. Within the two-phase region, the structural parameters ascribed to the both phases gradually increase and above 420–430 °C the compound becomes single phase with the non-polar orthorhombic structure. The obtained results are in accordance with those described in Ref. [10]. It should be noted that the variation in the unit cell volumes calculated for the compounds with  $x = 0.11$  and  $x = 0.13$  is nearly double as compared to that observed for the  $x = 0.15$  sample and for the pristine BiFeO<sub>3</sub> [29]. This difference is most probably caused by different routes of the phase transition and related more significant structural changes occurred in these compounds as compared with those estimated for the  $x = 0.15$  sample.

The anomaly observed in the DSC curves of the  $x = 0.11$  and  $x = 0.13$  compounds is significantly less than that observed in the  $x = 0.15$  sample [10] and reflects the difference in the structural phase stable near the phase transition. The DSC data testify quite small amount of enthalpy associated with the structural transition occurred in the compounds with  $x = 0.11$  and  $x = 0.13$  as compared to those obtained for the 15% doped compound and pristine bismuth ferrite (Fig. 3) [10]. The results of differential thermal analysis confirm the difference in the background of the structural transition occurred in the compound with  $x = 0.11$  and  $x = 0.15$  and pristine bismuth ferrite. Analysis of the crystal structure evolution as well as the DSC data obtained for the  $x = 0.11$ , 0.13 and  $x = 0.15$  compounds points at the fact that the dominant amount of the rhombohedral phase

significantly facilitates the structural transition into the non-polar orthorhombic phase.

The obtained results indicate a quite complex nature of the structural transition to the non-polar orthorhombic state observed for the compound with  $x = 0.11$ . Careful analysis of the diffraction patterns at the temperature prior to the formation of the non-polar orthorhombic phase ( $\sim 450$  °C) allowed the authors to reveal tiny peaks attributed to the anti-polar orthorhombic phase (inset to the Fig. 1, pattern recorded at 425 °C for  $2\theta$  region about 33°); above this temperature, the structure can be successfully refined using the centrosymmetric space group Pnma. In order to clarify the observed structural peculiarities, the authors have performed the high-resolution transmission electron microscopy measurements (HRTEM).

The HRTEM investigations have been performed in the temperature range 20–700 °C. The HRTEM images shown in Fig. 4 were obtained on a single crystal grain with a size of approximately 100 nm. The FFT images calculated for this region at temperatures above room temperature testify the pattern specific to the rhombohedral phase described by  $R3c$  space group with (001) zone axis orientation. The FFT image calculated for the temperature of 450 °C reveals the appearance of new pair of spots corresponding the plane distances  $d \approx 3.9$  Å in real space

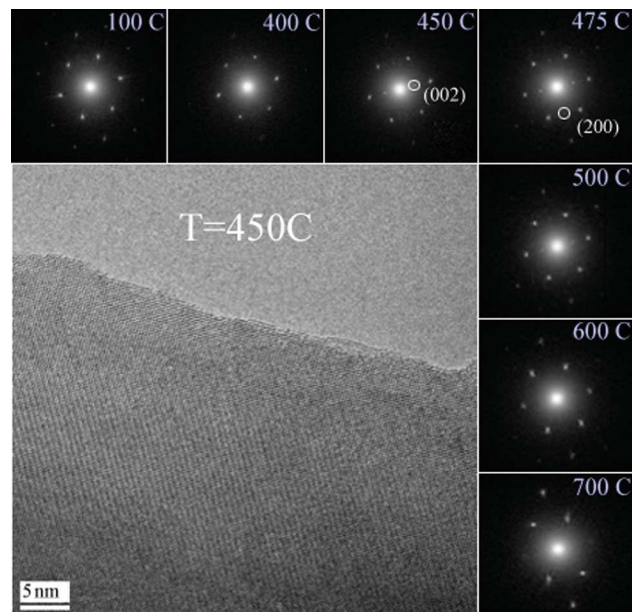


**Figure 4** HRTEM image of the compound with  $x = 0.11$  at  $T = 450$  °C. The insets show FFT images calculated for the temperature region 100–700 °C.

and can be associated with (002) reflection attributed to the anti-polar orthorhombic phase (for the compound with  $x = 0.13$ , the related reflections can be observed at  $2\theta \approx 22.7$ , Fig. 2). The FFT performed for the temperature of about  $\sim 475$  °C testifies the appearance of new two maximums at  $d \sim 2.8$  (Fig. 4) that correspond to (200) reflection which can be observed on the diffraction pattern at  $31.7^\circ$  (Fig. 2). The appearance of the non-polar orthorhombic phase detected by HRTEM data explicitly confirms the results of the conventional X-ray diffraction measurements. The spots attributed to the anti-polar orthorhombic structure is observed at temperatures up to 500 °C, and further temperature increase leads to a stabilization of the non-polar orthorhombic structure (the FFT image calculated for the  $T = 700$  °C can be successfully simulated using the orthorhombic lattice described by *Pbnm* space group with (010) zone axis orientation). It should be noted that the X-ray diffraction pattern recorded at  $T = 500$  °C has been already refined assuming the single-phase structural state within the non-polar orthorhombic phase (*Pbnm* space group). The variations in the temperature ranges estimated for the mentioned structural phase can be explained by a difference in the evolution of the crystal structure estimated by microscopic and local scale measurements.

## Conclusions

The temperature- and composition-driven structural transitions in the  $\text{Bi}_{1-x}\text{Pr}_x\text{FeO}_3$  ceramics of the compositions within the phase coexistence region have been studied with X-ray diffraction and transmission electron microscopy measurements. The structural analysis has clarified the morphotropic phase boundary region existed in the range of  $0.11 \leq x \leq 0.15$  at room temperature. The obtained data have also specified the temperature-driven structural transition into the non-polar orthorhombic phase depending on the initial structural state of the compounds. The structural peculiarities have been followed depending on the phase ratio at room temperature. The structural data have determined a revival of the anti-polar orthorhombic phase with increasing temperature prior to the formation of the non-polar orthorhombic phase. Specific role of the anti-polar phase acting as a mediator between the

polar rhombohedral and the non-polar orthorhombic phases across the temperature- and composition-driven phase transition has thus been considered.

## Acknowledgements

The authors would like to acknowledge the BRFFR (Grant F16R-066), JINR-BRFFR (Grant F16D-008), RFBR (Grant 16-58-00082) and MK-1720.2017.8. V. A. K. is grateful to Fundação para a Ciência e a Tecnologia for financial support through the FCT Investigator Programme (Project IF/00819/2014). The work done at University of Aveiro was supported by the project TUMOCS. This project has received funding from the European Union's Horizon 2020 research and innovation programme under the Marie Skłodowska-Curie Grant No. 645660.

## References

- [1] Yuan GL, Or SW, Liu JM, Liu ZG (2006) *Appl Phys Lett* 89:052905–052907
- [2] Chen X, Hu G, Wu W, Yang C, Wang X (2010) *J Am Ceram Soc* 93:948–950
- [3] Troyanchuk IO, Karpinsky DV, Bushinsky MV, Khomchenko VA, Kakazei GN, Araujo JP, Tovar M, Sikolenko V, Efimov V, Kholkin AL (2011) *Phys Rev B* 83:054109–054115
- [4] Troyanchuk IO, Karpinsky DV, Bushinsky MV, Mantyskaya OS, Tereshko NV, Shut VN (2011) *J Am Ceram Soc* 94:4502–4506
- [5] Cheng C-J, Kan D, Anbusathaiah V, Takeuchi I, Nagarajan V (2010) *Appl Phys Lett* 97:212905-1–212905-3
- [6] Kan D, Palova L, Anbusathaiah V, Cheng CJ, Fujino S, Nagarajan V, Rabe KM, Takeuchi I (2010) *Adv Funct Mater* 20:1108–1115
- [7] Levin I, Tucker MG, Wu H et al (2011) *Chem Mater* 23:2166–2175
- [8] Khomchenko VA, Troyanchuk IO, Bushinsky MV, Mantyskaya OS, Sikolenko V, Paixão JA (2011) *Mater Lett* 65:1970–1972
- [9] Karpinsky DV, Troyanchuk IO, Tovar M, Sikolenko V, Efimov V, Efimova E, Shur V Ya, Kholkin AL (2014) *J Am Ceram Soc* 97:2631–2638
- [10] Karpinsky DV, Troyanchuk IO, Sikolenko V, Efimov V, Efimova E, Willinger M, Salak AN, Kholkin AL (2014) *J Mater Sci* 49:6937–6943
- [11] Karpinsky DV, Troyanchuk IO, Tovar M, Sikolenko V, Efimov V, Kholkin AL (2013) *J Alloys Compd* 555:101–107

- [12] Karpinsky DV, Troyanchuk IO, Mantytskaja OS et al (2014) *Phys Solid State* 56:701–706
- [13] Karpinsky DV, Troyanchuk IO, Zheludkevich AL, Ignatenko OV, Silibin MV, Sikolenko VV (2016) *Phys Solid State* 58:1590–1595
- [14] Karimi S, Reaney I, Han Y, Pokorny J, Sterianou I (2009) *J Mater Sci* 44:5102–5112
- [15] Arnold D (2015) *IEEE Trans Ultrason Ferroelectr Freq Control* 62:62–82
- [16] Minh NVT, Dao Viet (2010) *J Nonlinear Opt Phys Mater* 19:247–254
- [17] Mahato DK, Saha S, Sinha TP (2016) *J Phys Chem Solids* 92:45–52
- [18] Trivedi P, Katba S, Jethva S et al (2015) *Solid State Commun* 222:5–8
- [19] Banerjee P, Franco A (2016) *J Mater Sci Mater Electron* 27:6053–6059
- [20] Shivanand M, Swarup K, Rajasekhar B, Varma KBR (2016) *Mater Res Express* 3:065009–065015
- [21] Srivastav SK, Gajbhiye NS, Banerjee A (2013) *J Appl Phys* 113:203917-1–203917-6
- [22] Karpinsky DV, Troyanchuk IO, Pushkarev NV et al (2015) *J Alloys Compd* 638:429–434
- [23] Rodríguez-Carvajal J (1993) *Phys B* 192:55–69
- [24] Khomchenko VA, Troyanchuk IO, Karpinsky DV, Paixao JA (2012) *J Mater Sci* 47:1578–1581. doi:[10.1007/s10853-011-6040-4](https://doi.org/10.1007/s10853-011-6040-4)
- [25] Rusakov DA, Abakumov AM, Yamaura K, Belik AA, Van Tendeloo G, Takayama-Muromachi E (2010) *Chem Mater* 23:285–292
- [26] Teslic S, Egami T (1998) *Acta Cryst B* 54:750–765
- [27] Zhang J, Wu Y-J, Chen X-J (2015) *J Magn Magn Mater* 382:1–6
- [28] Kumar N, Panwar N, Gahtori B, Singh N, Kishan H, Awana VPS (2010) *J Alloys Compd* 501:L29–L32
- [29] Selbach SM, Tybell T, Einarsrud M-A, Grande T (2008) *Adv Mater* 20:3692–3696